

Seeing the wood through the trees. Combining shape information from different landmark configurations

Type

Research paper

Keywords

geometric morphometrics, morphology, skull, primates, 2D images, combinland

Abstract

The geometric morphometric (GM) analysis of complex anatomical structures is an ever more powerful tool to study biological variability, adaptation and evolution. Here, we propose a new method (combinland), developed in R, meant to combine the morphological information contained in different landmark coordinate sets into a single dataset, under a GM context. combinland builds a common ordination space taking into account the entire shape information encoded in the starting configurations. We applied combinland to a Primate case study including 133 skulls belonging to 14 species. On each specimen, we simulated photo acquisitions converting the 3D landmark sets into six 2D configurations along standard anatomical views. The application of combinland shows statistically negligible differences in the ordination space compared to that of the original 3D objects, in contrast to a previous method meant to address the same issue. Hence, we argue combinland, allows to correctly retrieve 3D-quality statistical information from 2D landmark configurations. This makes combinland a viable alternative when the extraction of 3D models is not possible, recommended, or too expensive, and to make full use of disparate sources (and views) of morphological information regarding the same specimens. The code and examples for the application of combinland are available in the Arothron R package.

Explanation letter

Dear Editor,

We wish to thank you and the reviewers for the insightful comments were given in order to improve our manuscript. We managed to answer to all of the concerns to accommodate the suggestions received.

The manuscript is not under consideration by any other journal and has not been previously published or sent out for review elsewhere. All authors have approved the manuscript and agree with its submission to the journal.

With best regards,

Antonio Profico

[Replies and Cover Letter.pdf](#)

1 **Seeing the wood through the trees. Combining shape information from**
2 **different landmark configurations**

3 Antonio Profico^{1*}, Paolo Piras², Costantino Buzi¹, Antonietta Del Bove^{3,4}, Marina Melchionna⁵,
4 Gabriele Senczuk⁶, Valerio Varano⁷, Alessio Veneziano⁸, Pasquale Raia⁵, Giorgio Manzi¹

5
6 1 - Dipartimento di Biologia Ambientale, Sapienza Università di Roma, Rome (Italy)

7 2 - Scienze cardiovascolari, respiratorie, nefrologiche, anesthesiologiche e geriatriche, Sapienza
8 Università di Roma, Rome (Italy)

9 3 - Catalan Institute of Human Paleoecology and Social Evolution (IPHES), Tarragona (Spain)

10 4 - Àrea de Prehistòria, Facultat de Lletres, Universitat Rovira i Virgili, Tarragona (Spain)

11 5 - Dipartimento di Scienze della Terra, dell'Ambiente e delle Risorse, Università di Napoli, Federico
12 II, Naples (Italy)

13 6 - Dipartimento di Biologia e di Biotecnologia, Sapienza Università di Roma, Rome (Italy)

14 7 - Dipartimento di Architettura, Università degli Studi di Roma Tre, Rome (Italy)

15 8 - School of Natural Sciences and Psychology, Liverpool John Moores University, Liverpool (United
16 Kingdom)

17
18 26 pages, 11 figures, 6 tables.

19 Running title: *combinland*: a method to combine 2D landmark sets

20
21 Dr. Antonio Profico

22 Dipartimento di Biologia Ambientale, Sapienza Università di Roma, P.le Aldo Moro 5, 00185 Roma

23 +390649912690

24 antonio.profico@uniroma1.it

25

26
27

ABSTRACT

The geometric morphometric (GM) analysis of complex anatomical structures is an ever more powerful tool to study biological variability, adaptation and evolution. Here, we propose a new method (*combinland*), developed in R, meant to combine the morphological information contained in different landmark coordinate sets into a single dataset, under a GM context. *combinland* builds a common ordination space taking into account the entire shape information encoded in the starting configurations. We applied *combinland* to a Primate case study including 133 skulls belonging to 14 species. On each specimen, we simulated photo acquisitions converting the 3D landmark sets into six 2D configurations along standard anatomical views. The application of *combinland* shows statistically negligible differences in the ordination space compared to that of the original 3D objects, in contrast to a previous method meant to address the same issue. Hence, we argue *combinland*, allows to correctly retrieve 3D-quality statistical information from 2D landmark configurations. This makes *combinland* a viable alternative when the extraction of 3D models is not possible, recommended, or too expensive, and to make full use of disparate sources (and views) of morphological information regarding the same specimens. The code and examples for the application of *combinland* are available in the *Arothron* R package.

Keywords: 2D images; geometric morphometrics; primates; skull; morphology.

Graphical abstract

“*combinland*” is a new method to combine the morphological information coming from different landmark coordinate sets acquired on different configurations. These configurations can be different 2D views of a 3D object or even a mix of 2D and 3D configurations. “*combinland*” is a feasible alternative when the extraction of complete 3D models is not possible.

54 INTRODUCTION

55 Ever since Blumenbach (1865) the study of cranial morphology makes use of linear measurements
56 allowing to compare individuals and species. The later development of geometric morphometrics (GM)
57 paved the way for the study of morphological variation avoiding to reduce ‘shape’ down to a set of
58 linear measurements (or ratios) of some sort (Rohlf, 2000). Geometric morphometrics is much more
59 accurate of linear measurements as a shape descriptor. Consequently, GM represents the most common
60 method to quantify size and shape variations in biological and paleobiological applications (Rohlf and
61 Marcus, 1993; Jungers *et al.*, 1995; Adams *et al.*, 2004, 2013; Piras *et al.*, 2009, 2010, 2014; Sansalone
62 *et al.*, 2015; Neaux *et al.*, 2018).

63 Under GM, either two- (2D) or three-dimensional (3D) configurations of landmarks are recorded. The
64 former (2D) approach relies on the pictorial representation of the biological objects of interest (e.g.
65 pictures, X-ray, MRI) (Bastir and Rosas, 2009, 2006; Adams *et al.*, 2004; DeQuardo *et al.*, 1999),
66 whereas the latter works by recording the landmarks directly on the three-dimensional object, as
67 represented by either the real item of interest (i.e. using 3D digitizers) or by digital reconstructions
68 acquired through computer tomography, laser scanning, or photogrammetry (Profico *et al.*, 2018; Olsen
69 and Westneat, 2015; Weber, 2015; Bates *et al.*, 2010). One major advantage of 2D over 3D data is that
70 they are more easily acquired visiting museum collections or any other repository and a wealth of 2D
71 data (pictures) are readily available online through published sources. The acquisition of 2D data is fast
72 and relatively inexpensive, so that sample size almost always rises above those typical for 3D studies.
73 During the last decades the increased availability of 3D digital repositories is spurring interest on 3D
74 geometric morphometrics (Cardini, 2014; Davies *et al.*, 2017). This is welcome since the morphological
75 information that comes with 3D objects is richer and more genuine than with 2D samples, which suffers
76 from shape distortion due the ‘parallax problem’ (Mullin and Taylor, 2002), and are further limited to
77 a single view of the objects of interest (Ponton, 2006). Unfortunately, the acquisition of 3D data is still
78 expensive and time-consuming (Cunningham *et al.*, 2014). Moreover, 3D models often require post-
79 production to refine the quality of the digital specimens (e.g. decimation and smoothing procedures,
80 Veneziano *et al.*, 2018) which further lengthens the data processing time.

81 In this study, we propose a new statistical approach which combines multiple 2D datasets into
82 a unique matrix that can be subjected to ordination analyses encoding the whole morphological
83 information. The most straightforward way to test this tool is the recovery of 3D morphological
84 information starting from different 2D views. It must be emphasized, though, that our approach can be
85 used to combine different 2D or 3D configurations or even 2D and 3D configurations together. It is
86 similarly important to remark that our purpose is *not* to build the 3D geometry via single 2D views, as
87 done by photogrammetry. Instead, we want to build a common ordination space starting from shapes
88 acquired with different number of landmarks in both 2D or 3D.

89 The method (“*combinland*”), is based on a technique originally proposed by Adams (1999).
90 *combinland* works by merging the morphological information obtained from the Generalized Procrustes
91 Analysis (GPA) of different datasets into a single matrix of coordinates. Differently from the traditional
92 method (Adams, 1999; Davis *et al.*, 2016; Meloro *et al.*, 2017), in *combinland* we introduced a new
93 size correction to guarantee a proper combination of multiple landmark configurations weighting sizes
94 for the number of landmarks and dimensions. In addition, in *combinland* we supply a solution to
95 calculate and plot the shape variations of each combined landmark configuration associated to the
96 extreme values of the PC scores, in keeping with the issue of improving the visualization of shape
97 changes in GM applications (Klingenberg, 2013). We assessed the performance of *combinland* using a
98 3D dataset from which we derived six 2D datasets (referring to specific anatomical views) to assess
99 whether the combined 2D information compares well to 3D data, considered as “ground truth”. We
100 provide the R code, embedded in the *Arothron* R package (Profico *et al.*, 2019), to apply *combinland*
101 to 2D datasets.

104 MATERIALS AND METHODS

105 *3D and 2D datasets: the Primate case study*

106 We sampled in 3D, 55 landmarks (Supp. Fig. 1) over the cranial surfaces of 14 Primate species
107 belonging to Catarrhini (10 species) and Platyrrhini (4 species) for a total of 133 specimens (see Supp.

Table 1 for details). Starting from the 3D objects, we produced six 2D datasets for each specimen, defined along the six main anatomical views (i.e., frontal, superior, inferior, posterior, right lateral and left lateral) used in anthropology, which refer to the midsagittal and the Frankfurt planes, respectively. The midsagittal plane is defined by the *prosthion*, *bregma* and *basion* anatomical points. The Frankfurt plane is defined by different points (here digitized as landmarks): the left *orbital* (intended as the lowest point on the orbital rim) and both left and right *poria*. The left- and the right-lateral 2D sets (1-2) are defined by projecting the 3D coordinates orthogonally onto the midsagittal plane, the superior and the inferior sets (3-4) are obtained projecting the 3D set onto the Frankfurt plane. Finally, the posterior and the anterior sets (5-6) are calculated in two steps: *i*) the rotation of the Frankfurt plane of $\pi/2$ radians and *ii*) projection of the 3D coordinates on the plane.

By using 3D digital models, visible landmarks can be defined with respect to a point of view (POV) external to the object. Straight lines are projected from the POV coordinates towards each landmark. If the projection line intersects the 3D object external surface before reaching the landmark, the latter is defined as non-visible, or visible otherwise. The method, referred to as CA-LSE (Computer Assisted Laser Scanner Emulator) is described in Profico and colleagues (2018b, see Fig. 1).

After defining 2D landmarks configurations, we performed a Generalized Procrustes Analysis (GPA), without scaling, on each 2D set. The third dimension was intentionally set to zero in such configurations, as it happens when taking digital pictures of the specimens. The procedure is summarized in Figure 1. We obtained six 2D datasets of landmark in left-lateral (N=24), right-lateral (N=24), superior (N=17), inferior (N=40), posterior (N=16) and anterior (N=20) anatomical views (see Supp. Fig. 2 and Supp. Table 2). It is crucial to note here that our conversion from 3D into six 2D configurations does not realistically mimic the 2D photo acquisition of an osteological collection from the different anatomical views. Our procedure does not simulate the potential effect of Parallax problem due to the distortion or lens positioning intrinsically present in photographs (see Discussion section).

[Figure 1]

The “combinland” method

Under “*combinland*” separate GPAs are performed for each 2D anatomical view, separately, and scaled to the unit Centroid Size (CS). In geometric terms the CS represents the quadratic mean of the projections, along each the m coordinate directions, of the vector difference between each landmark and the centroid. At this stage, the 2D datasets are not comparable. In fact, CS cannot be used to compare sizes of shapes identified by different number of landmarks. A convenient way to normalize the CS (size correction) is to divide it by the square root of the number of landmarks times the number of dimensions (as suggested in Dryden and Mardia 2016, section 2.2.2). This quantity gives the quadratic mean squared distance of the landmarks to their centroid, i.e. the $k * m$ components (where k is the number of landmarks and m is that of dimensions) of the centred configuration matrix. The six corrected (by the number of landmarks) matrices of aligned coordinates are appended together to compose a single matrix (2DComp), which is then subjected to principal component analysis (PCA). The PC scores extracted from 2Dcomp represent the descriptors of the whole morphological variation in the combined 2D data. The procedure is summarized in Figure 2.

In sum, the protocol applied herein consists of 5 steps: i) capturing the 2D landmark configurations according to the six standard anatomical views, ii) performing a GPA on each of the six 2D datasets, iii) applying “size correction” to the six sets of aligned coordinates derived from GPA: this size correction consists in re-multiplying coordinates (that were originally divided by their proper CS) by the square root of their number of landmarks (that vary among different configurations) times their number of dimensions (that in this specific case is always 2, see below), iv) appending the six matrices of corrected coordinates, v) performing PCA on the new data matrix. Points ii to v represent *combinland*.

To visualize the shape variations for each of the six 2D views associated to the combined data we used: i) the mean shapes corresponding to 2D datasets of the coordinates after GPA. The coordinates of these mean shapes are re-multiplied by the square root of the number of landmarks of the corresponding 2D view times the number of dimensions. ii) the sub-matrix corresponding to those landmarks belonging to a particular 2D view from the eigenvalue matrix coming from the PCA performed on the combined (size-corrected) 2D coordinates corresponding only to the 2D landmarks set that is needed for visualization. iii) the values of the PC scores for which the visualization is called.

170 162 [Figure 2]

171 163 We also compared the shape variations predicted by 3D PCA with those coming from
172 164 *combinland* PCA projecting the PCA-predicted 3D shapes on the same planes used to obtain 2D
173 165 landmark sets. To assess the differences between the shape variations coming from 3D data and those
174 166 from 2D combined data we calculated the Procrustes Distances between the projections of shapes
175 167 predicted by PCA on true 3D data and those coming from PCA on combined 2D data.

177 169 *Geometric morphometrics, centroid size and biological implications*

178 170 Size variability affects shape variation in biological structures. Under GM shape is defined as ‘*the*
179 171 *geometric information that remains when location, scale and rotational effects are filtered out from*
180 172 *an object*’ (Kendall, 1977). In turn, such geometric information is defined by the acquisition of the
181 173 coordinates of landmarks corresponding to homologous anatomical points. The Generalized
182 174 Procrustes Analysis (Gower, 1975) removes the information of the components of location, scaling
183 175 and rotational. The size component is habitually defined as the square root of sum of the squared
184 176 distances between landmarks and the centroid of the configuration (Bookstein, 1989). According to
185 177 Bookstein (1986) CS is therefore uncorrelated with shape under the assumption that the variation
186 178 around each landmark mean is represented by small, independent, identically distributed circular
187 179 normal errors. However, this assumption cannot account for the true error distributions and thus there
188 180 is no inherently best size measure. In continuum mechanics, for example, the m-Volume is the most
189 181 used size measure (Varano *et al.*, 2018) as it is specifically related to a physical domain of the body
190 182 under study (m-Volume has a unit of measurement, CS does not), a concept that could become very
191 183 elusive when dealing with single digitization of points sparse in complex structures. The mathematic
192 184 formulation of CS pretends it is correlated to the “actual size” of the anatomical traits. However, any
193 185 size measure should reflect the true physical size of the object under study. It follows that identical
194 186 structures, digitized in different ways, should have or identical or approximately equal sizes.
195 187 Nevertheless, the value of CS is influenced by the total number of landmarks defining the shape and
196 188 the contribute made by each landmark is proportional to its squared distance to the centroid (Fig. 3).

189 [Figure 3]

190 As it stands, the CS increases with increasing number of landmarks and is influenced by the squared
 191 distance of landmarks to the centroid. Under conventional GM studies this is not relevant, because the
 192 same configuration applies to all specimens. Yet, it becomes relevant when combining different
 193 configurations. To fix this problem, we propose a different solution from Adams (1999) and Davis
 194 and colleagues (2016), by computing the relative size of different norms in reference to the total
 195 dimension of the considered norms. In particular, Adams (1999) and Davis *et al.*(2016) combine two
 196 different views (F and S) each with their proper size CS_F and CS_S of a digitized structure into a single
 197 dataset that parameterizes the single sizes on their sum (formula 1):

$$CS^F = \left[\frac{CS_F}{CS_F + CS_S} \right],$$

$$CS^S = \left[\frac{CS_S}{CS_F + CS_S} \right],$$

200 where upper scripts F and S correspond respectively to the F and S *relative* components of the
 201 centroid size (CS).

202 Defining each anatomical view as $k * m$, where k is the number of landmarks and m is the number of
 203 dimensions (2D or 3D) we divided the CS by \sqrt{km} (as proposed in Dryden and Mardia 2016, section
 204 2.2.2) :

$$CS^F = CS_{F} / \sqrt{K_F m_F}$$

$$CS^S = CS_{S} / \sqrt{K_S m_S}$$

208 A simple simulation proves this point. We digitized two circle outlines placing 10- and then 100
 209 landmarks, respectively (Fig. 4a,b). From each configuration, we generated 300 landmark-wide
 210 configurations using the Dryden-Mardia (2016) model (Fig. 4) and calculated the mean relative sizes
 211 of each configuration using either our CS correction (formula 2) or using *combine.subsets()* (formula

[Download source file \(111.24 kB\)](#)

1) function in geomorph package (Adams and Otárola-Castillo, 2013) which is based on the approach of Davis et al. (2016).

[Figure 4]

By using our method, the relative CS for the two datasets are both equal to 0.50. The mean values of the relative CS after the application of the formula 2 (Davis *et al.*, 2016) are equal to 0.24 and 0.76 respectively.

A simulated example

A simulated example shows the efficacy of *combinland* CS correction. We started by producing two 2D configurations with a different number of landmarks. The first dataset is defined starting from an “irregular polygon shape” configuration, the second one from a “circular shape” configuration. On these shapes we applied non-affine deformation cycles (Piras et al. 2016). The cycles apply a combination of aspect ratio and bending. This way, we produced 2D datasets of shapes each with 10 and 200 landmarks from the “irregular” and “circular” shapes respectively. Successively, we converted the 2D shapes into 3D landmark configurations adding a third dimension each, perpendicularly to the x - y and x - z planes respectively, for the two configurations, centred at the origin (Fig. 5).

[Figure 5]

From the 2D datasets, we thus have i) a combined version with the size correction (*combinland*), ii) a combined version without size correction iii) a 3D dataset. For each of the three datasets we performed a PCA after Procrustes registration. In Figure 6 we reported the three resulting PCA plots.

[Figure 6]

In order to compare the PCA spaces we adopted the same strategy used in Varano et al (2017): we calculated the Riemannian distance between the shapes identified by the scores of the first two PC

236 scores (Figure 6). These shapes are approximately elliptical. In each of the three analyses the first two
237 PC scores summarize approximately 97% of total variance. The Riemannian distances between the
238 shapes identified by the first two PC scores of the 3D dataset and those identified by the first two PC
239 scores of the combined 2D datasets using *combinland* is 0.008. This same distance rises to 0.060
240 without correction. Eventually, we calculated the geodesic distance of the UPGMA cluster built using
241 the first two PC scores coming from 3D dataset with those coming from the two combined 2D
242 datasets (see Supp. Fig. 3), i.e. with and without size correction; they are equal to 0.27 and 5.87
243 respectively. Fig. 7 shows the shapes predicted at max and min values of PC1 and PC2 for the two
244 substructures as predicted by combining the data with size correction, without size correction and on
245 3D data, respectively, showing how close the size-corrected data come to 3D. A Mantel test
246 performed between the PC scores coming from the 3D dataset and those of PCA that uses *combinland*
247 is equal to 1. The same test performed between the 3D dataset and the PC scores from combined 2D
248 data without applying the size correction returns a value equal to 0.95. Although apparently minimal,
249 this result confirms the appropriatedness of the size correction procedure.

[Figure 7]

251 This result is further confirmed by the calculation the Procrustes distances between the shape
252 variations from 3D data and those calculated from the 2D data with and without the size correction
253 (Table 1). The difference between the shape variations from 3D and combined 2D data with size
254 correction calculated at the extremes of the first two PC scores are negligible (Table 1).

[Table 1]

Evaluation of combinland performance on Primate skulls

258 To assess the performance of *combinland* in the real Primate skull case, we compared the PCA
259 coming from the 3D data (3D data) with the PCA on the 2D data processed under *combinland* and under
260 the strategy without size correction.

273 261 The PC scores of the entire shape of all datasets (3D and 2D) were subjected to cluster analysis
274 262 using the Unweighted Pair Group Method with Arithmetic mean (UPGMA, Sokal and Michener, 1958).
275 263 We defined and combined two categorical variables for each specimen: species and gender. By using
276 264 UPGMA trees, we checked how well the 2D data reproduces the 3D trees topology. The use of phenetic
277 265 trees to assess *combinland* performance is crucial because the error introduced using 2D data to
278 266 represent 3D objects can be as large as the shape distance between two species (Cardini, 2014). The
279 267 similarity between 2D and 3D clusters was quantified by using both the geodesic and the edge set
280 268 distances. The geodesic distance is the sum of the difference between the corresponding path between
281 269 two weighted phylogenetic trees. The edge set distance is computed as sum of the differences between
282 270 the number of internal branches and/or inversions between two weighted phylogenetic trees (Chakerian
283 271 and Holmes, 2012; Owen and Provan, 2011).

284 272 We scaled the edge length of the trees by imposing an equal (arbitrarily unitary) total edge
285 273 length. The six anatomical views can be combined into smaller subgroups of size n (where n represents
286 274 the number of 2D views combined together). For $k =$ six anatomical views there are $2^k - 1 = 63$ possible
287 275 combinations of 2D sets (from the six each with only one configuration to the one including all of them).
288 276 We produced 63 UPGMA-based cluster analyses, one for each of the 63 possible combinations.
289 277 Subsequently, we calculated for each of the 63 UPGMA trees the geodesic and the edge set distance
290 278 from the UPGMA tree built using the PC scores of the 3D data. Eventually, we evaluated the covariation
291 279 between the PC scores coming from the 3D and 2D data (with and without landmark's number
292 280 correction) by Partial Least Squares (PLS) analysis (Rohlf and Corti, 2000).

293 281 In addition, we performed the Mantel test between the matrix of PC scores of the 3D data and
294 282 the PC scores of the combined 2D data (with and without the "size correction") appending the two,
295 283 three, four, five and six anatomical views generating all the 57 possible combinations.

296 284 We further evaluated *combinland* performance by comparing the shape variation explained by
297 285 3D PCA with those explained by the combined 2D sets. In detail, we produced six bi-dimensional
298 286 projections of 3D shape variations predicted at positive and negative extreme values of the PC scores,
299 287 applying the same projection protocol used to create the 2D datasets.

288 We also compared the eigenvectors coming from separate PCA performed on these two arrays:
289 the first one is related to the shape variations associated to the extreme values (minimum and maximum)
290 of the first three PC scores of the 2D data; the second one refers to the shape variations of the 3D dataset
291 projected into two-dimensional Cartesian system. This analysis aims at verifying whether, besides
292 correlation between scores, the morphologies explained by the ordination methods are actually similar.
293 In addition, we combined these two types of arrays into one and we performed a PCA. 3D and 2D
294 shapes corresponding to the same PC extremes should result in “coupled” data. We also performed an
295 analysis of evolutionary allometry in Platyrrhini, Cercopithecoidea, Hominoidea evaluating the effect of
296 the same size regressor (CS from 3D data) on the shape from 3D and 2D datasets (with and without
297 “size correction”).

298 Eventually, we compared the shapes of each specimen from the 3D PCA with those obtained
299 from the combined 2D analyses. The two datasets consist on the shapes identified by the first 20 PCs
300 in the PC space of the corresponding analyses (explaining collectively more than 95% of total variance).
301 From the 3D PCA, we calculated for each specimen six bi-dimensional shapes using the six anatomical
302 views used in the combined 2D analyses. To quantify the differences between them, we calculated the
303 partial Procrustes distance normalized on the maximum distance allowed (that is $\sqrt{2}$, Varano *et al.*
304 2017).

308 RESULTS

310 *Principal Component Analysis on 3D and 2D data*

311 The first two PC scores of the 3D and 2DComp data explain together the 53.21% and the 51.45%,
312 respectively, of the total variance (Fig. 8). In the two plots (3D and 2D) the Cercopithecoidea (*Macaca*,
313 *Papio* and *Theropithecus*) are located on the positive value of the PC1 close to the great Apes (*Pan*,
314 *Gorilla* and *Pongo*). New World monkeys (*Cebus*, *Ateles* and *Alouatta*) and hylobatids (*Hylobates* and

315 *Symphalangus*) occur at the negative values of the PC1. Along PC2 there is a clear distinction between
316 the group formed by *Pongo* and *Alouatta* from all other species (Fig. 9).

317 [Figure 8]

318 [Figure 9]

319 The morphological variation associated to the first two PCs of 3D and combined 2D analyses
320 are very similar (Fig. 10). From the anterior view, the pattern of shape variation along the PC1 is
321 associated with the maximum height of the face and the relative shape and position of the piriform
322 aperture: along positive values the face and the nasal aperture are high. PC2 is mainly associated to
323 facial width: at positive values the facial complex broadens (Fig. 10). From the posterior view, PC1
324 captures variation associated to the position of the *poria*. PC2 records the relative positions of *bregma*
325 and *asteria*. Still, a change associated to the orientation of the foramen magnum seems discriminating
326 among specimens (Fig. 10). In lateral view, PC1 captures the rate of the alveolar prognathism. Along
327 PC2, shape changes associate to the degree of airorhynchy (Fig. 10).

328 [Figure 10]

329 From the superior view the most prominent shape changes relate to the lengthening of the
330 skull (PC1) and to the relative position of the supraorbital region (PC2). At positive values of PC1 the
331 supraorbital region appears shifted posteriorly (Fig. 10).
332 Along PC1, from the inferior view, shape changes is associated the anterior shifting of the *foramen*
333 *magnum* is well distinct at positive values of this vector. PC2 records the relative size of the occipital
334 bone, that is broader at positive values. Also, the relative size of the *foramen magnum* is affected: at
335 positive values it appears broader than at negative values (Fig. 10). These results indicate that
336 *combinland* provides realistic shape variation information as compared with the 3D data, at least when
337 6 different views are combined together.

339 ***Performance of the combinland method***

340 The geodesic and edge set distances calculated on the UPGMA trees (Supp. Fig. 4-5) produced
341 by using the PC scores are smaller when the correction for the number of landmarks is applied (Table
342 2) indicating such correction is appropriate.

[Download source file \(111.24 kB\)](#)

[Table 2]

As expected, the geodesic and the edge set distances between the original 3D sample and the combined 2D configurations decrease as number of anatomical views increases (Table 2). These distances are lower when the correction is applied and become negligible when at least 4 2D sets are combined.

[Figure 10]

PLS indicates that the morphological information of the two dataset types (2D and 3D), expressed in terms of vectors of PC scores, are close to each other. In fact, the correlation coefficients are close to 1 and the p-values are always significant. Correlation coefficients are higher for the 2Dcomp data with the size correction than without it (Table 3).

[Table 3]

The Mantel test performed between the first four PC scores of 3D data (more than 75% of the total explained variance) and those 2D data using *combinland* is equal to 0.99. The same test applied between the PC scores of 3D data and 2D combined data without “size correction” (Adams’ 1999 method) returns a value equals to 0.98. We performed also the Mantel test between the 3D data and 2D combined datasets (with and without size correction) appending all the 57 possible combinations by using six 2D datasets. The results are always better if size correction is applied (i.e., *combinland*) as reported in Table 4.

[Table 4]

After combining the 2D datasets we performed a Procrustes Anova, by using the function *procD.lm* of the *geomorph* R package, followed by pairwise comparisons of taxonomic groups (Hominoidea, Platyrrhines and Cercopithecoidea) to test for differences among groups in allometry. The shape variable consists of PC scores, the size variable (independent variable) consists on centroid sizes from 3D landmark configurations. Using 3D data or combined 2D data statistically significant differences between Cercopithecoidea-Platyrrhines and Hominoidea-Platyrrhines are always detected (Table 5). As shown in Figure 11 (bottom left) the shape variations associated with the first principal component at negative and positive extreme values of the 2D and 3D data are very close to each other. Eigenvectors

[Download source file \(111.24 kB\)](#)

386 370 corresponding to the first three PCs of separate PCA are contrasted in the scatterplot matrix in Fig. 11
387 371 bottom right.

388 372 [Figure 11]

389 373 The evolutionary allometry test quantifies the relative amount of shape information (PC scores)
390 374 attributable to covariation with size. The aim of this analysis is to evaluate the robustness of *combinland*
391 375 method when specific analyses are performed. We found the outputs coming from 3D and 2D combined
392 376 datasets close each other as reported in Table 5.

393 377 [Table 5]

394 378 The distances, expressed as percentage of the maximum distance allowed, between the shapes
395 379 identified by the first 20 PCs from the 3D data projected into two-dimensions and the 2D combined
396 380 datasets are low, indicating high correlation between the two datasets. The average distances of the full
397 381 sample expressed as percentage on each of the six anatomical views are 2.9% (anterior), 3.2%
398 382 (posterior), 0.7% (superior), 5.3% (inferior), 2% (left lateral) and 2% (right lateral) (see Supp. Table 3
399 383 for full results).

401 385 DISCUSSION

402 386 In landmark-based geometric morphometrics, shape variability is analysed through the definition of
403 387 homologous anatomical points. Such configuration of landmarks provides the best representation of
404 388 shape in the three dimensions. Nonetheless 2D data are much more common because they are easier to
405 389 collect and/or less expensive, and well-suited to deal with flat biological objects, like the hemimandibles
406 390 of vertebrates, the wings of insects and plants leaves (Meloro *et al.* 2015; Viscosi and Cardini 2011;
407 391 Klingenberg *et al.*, 1998). Herein, we present a new R tool which allows merging shape information
408 392 coming from different landmark sets. We proposed an example where different 2D views capture a 3D
409 393 biological object. Adams (1999) first introduced a method to combine sets of 2D shape variables
410 394 belonging to the same specimens. The relative sizes of the landmark configurations to be appended are
411 395 calculated as the ratio of the two subsets CS. This allows to accomplish a new PCA, but the visualization
412 396 of the shape variation associated to the new PC scores is somewhat complicated as a double step is

414 397 needed to resort the relationship between original 2D coordinates and the PC scores of the combined
415 398 analysis. Moreover, the ratio of CS values is not representative of the actual size differences between
416 399 configurations as a specific size correction that considers the number of landmarks and dimensions is
417 400 needed. The consequence of not performing such size correction is highly anecdotal as strongly
418 401 dependent on the type of configurations entering the analysis and their reciprocal size differences as
419 402 well as on the homogeneity of the spatial distribution of landmarks. Although this effect might be
420 403 negligible under most circumstances, it might become severe when the sizes of the configurations are
421 404 very different or when different sets are constituted by very different number of landmarks or when the
422 405 size and shape space is used during subsets GPAs. Since the introduction of semi-landmark in many
423 406 GM studies the morphology is acquired by using semi-landmarks homogeneously distributed along
424 407 curves or surfaces or on specific anatomical regions (e.g., supraorbital ridges, temporal lines, piriform
425 408 aperture). The use of semi-landmark is recommended when on the anatomical structures under
426 409 investigation none or a few of landmarks are detectable. Semi-landmark could be used in both 2D and
427 410 3D GM analyses. As stated in the “*Geometric morphometrics, centroid size and biological*
428 411 *implications*” section our proposed “size correction” mitigates the problem related when different sets
429 412 have a different number of landmarks. We did not use specifically semi-landmark sets in the real case
430 413 presented here. However, in the simulated GM example we show exactly what could happen when
431 414 combining two views composed by several landmarks as happens in semi-landmarks datasets. The
432 415 performance of *combinland* is better than “traditional” method proposed by Adams (1999) when the
433 416 number of landmarks of the combined configurations is different. We demonstrated that, given enough
434 417 2D information, *combinland* retrieves a relatively faithful representation of the morphological variation
435 418 of the ordination space obtained with 3D data.

436 419 We used *combinland*, on six 2D standard anatomical views for 133 skulls belonging to 14
437 420 different primate species, obtaining $133 \times 6 = 798$ 2D landmark configurations overall. We found that
438 421 both the general reciprocal position of species in the ordination plots and variance decomposition are
439 422 very similar to each other (Fig. 8-9). Furthermore, UPGMA built on PC scores pooled by species,
440 423 returned the same topological structure (edge set = 0, see Table 6) and very low geodesic distance

(1.34/100). The shape changes described by the PC scores calculated for the two sets (3D and 2D from *combinland*) are very close (Fig. 10). We showed that *combinland* replicates rather well the suite of morphological information encoded in original 3D data (Fig. 9 and (Supp. Fig. 7-11). When we asked how much 2D information is enough to gain the same insight, we found that using less than all anatomical views the results of 2D and 3D are qualitatively similar using six and four anatomical views (e.g., edge set distances from 3D results are equal to 59.00 and 67.73 respectively, for detail see Table 2). This is important because 2D information could not be as rich in real case studies as in our simulated one.

We therefore emphasize *combinland* could be safely used to re-process published data coming from two or more anatomical views of the same specimens (e.g. different bony elements), or as the final processing of data coming from photo shooting, originally designed for different purposes. This could be useful when dealing with fossilised remains where the acquisition of 3D data is not easily available (e.g. the Altamura man, Lari *et al.*, 2015), or even impossible given imperfect preservation.

In this study, we did not evaluate the influence of combining landmark data in order to face the integration and modularity between pre-defined modules. For example one could use *combinland* in order to build 2 views for defining one module and other two views for another. Then, exploring the covariation between these modules is matter for further investigations as we did not gauge this aspect here.

Also, as stated in the Introduction, our experiment here cannot simulate the Parallax problem present in real photographs (Mallison and Wings, 2014; Mullin and Taylor, 2002) due to either lens distortion or unperfect lens positioning relatively to the specimen. In fact, by using 3D digital models the projection of landmarks on specific planes (defined by triplets of points) is eased in comparison to the real life situation of dealing with photographic devices. A further study based on the comparison between results coming 3D data analysis and those from 2D analysis performed on data extracted from real photographs should expand upon the results we presented here in order to extend our knowledge about the performance of the procedure reported in this study. Moreover, the size correction is a standardization strategy aimed at yielding a reasonable approximation for comparing sizes. Given the

[Download source file \(111.24 kB\)](#)

470 451 very nature of CS, comparing sizes of different shapes constituted by landmarks digitized on an external
471 452 border only and on both external border and inner region could not be easy as it depends upon
472 453 landmark's spatial distribution.

474 455 **ACKNOWLEDGEMENTS**

475 456 We thank two anonymous reviewers for their help in improving the quality of the manuscript. We also
476 457 thank Andrea Cardini for useful suggestions and insights.

464 **REFERENCES**

465

466 Adams D.C., 1999. Methods for shape analysis of landmark data from articulated structures. *Evol.*

467

Ecol. Res. 1(8): 959–970.

468

Adams D.C., Otárola-Castillo E., 2013. Geomorph: An r package for the collection and analysis of

469

geometric morphometric shape data. *Methods Ecol. Evol.* 4(4): 393–399.

470

Adams D.C., Rohlf F.J., 2004. Slice DE. Geometric morphometrics: ten years of progress following

471

the ‘revolution.’ *Ital. J. Zool.* 71(1): 5–16.

472

Adams D.C., Rohlf F.J., Slice D.E., 2013. A field comes of age: geometric morphometrics in the 21st

473

century. *Hystrix, Ital. J. Mammal.* 24(1): 7–14.

474

Bastir M., Rosas A., 2006. Correlated variation between the lateral basicranium and the face: a

475

geometric morphometric study in different human groups. *Arch. Oral. Biol.* 51(9): 814–824.

476

Bastir M., Rosas A., 2009. Mosaic evolution of the basicranium in *Homo* and its relation to modular

477

development. *Evol. Biol.* 36(1): 57–70.

478

Bates K.T., Falkingham P.L., Rarity F., Hodgetts D., Purslow T., Manning P.L., 2010. Application of

479

high-resolution laser scanning and photogrammetric techniques to data acquisition, analysis and

480

interpretation in palaeontology. *Int. Arch. Photogramm. Remote Sens. Spat. Inf. Sci.* 38(5): 68–

481

73.

482

Blumenbach J.F., Bendyshe T., Marx K., Flourens P., Wagner R., Hunter J., 1865. The

483

Anthropological Treatises of Johann Friedrich Blumenbach... Anthropological Society.

484

Bookstein F.L., 1986. Size and shape spaces for landmark data in two dimensions. *Stat. Sci.* 1(2):

485

181–222.

486

Bookstein F.L., 1989. Size and shape: A comment on semantics. *Syst. Biol.* 38(2), 173–180.

487

Cardini A., 2014. Missing the third dimension in geometric morphometrics: how to assess if 2D

488

images really are a good proxy for 3D structures? *Hystrix, Ital. J. Mammal.* 25(2): 73–81.

- 510 489 Chakerian J., Holmes S., 2012. Computational tools for evaluating phylogenetic and hierarchical
511 490 clustering trees. *J. Comput. Graph. Stat.* 21(3): 581–599.
- 512 491 Cunningham J.A., Rahman I.A., Lautenschlager S., Rayfield E.J., Donoghue P.C.J., 2014. A virtual
513 492 world of paleontology. *Trends Ecol. Evol.* 29(6): 347–357.
- 514 493 Davies T.G., Rahman I.A., Lautenschlager S., Cunningham J.A., Asher R.J., Barrett P.M., Bates K.T.,
515 494 Bengtson S., Benson R.B.J., Boyer D.M., Braga J., Bright J.A., Claessens L.P.A.M., Cox P.G.,
516 495 Dong X.P., Evans A.R., Falkingham P.L., Friedman M., Garwood R.J., Goswami A., et al.,
517 496 2017. Open data and digital morphology. *Proc. R. Soc. B Biol. Sci.* 284(1852): 20170194.
- 518 497 Davis M.A., Douglas M.R., Collyer M.L., Douglas M.E., 2016. Deconstructing a species-complex:
519 498 Geometric morphometric and molecular analyses define species in the Western Rattlesnake
520 499 (*Crotalus viridis*). *PLoS One* 11(1): e0146166.
- 521 500 DeQuardo J.R., Keshavan M.S., Bookstein F.L., Bagwell W.W., Green W.D.K., Sweeney J.A., Haas
522 501 G.L., Tandon R., Schooler N.R., Pettegrew J.W., 1999. Landmark-based morphometric analysis
523 502 of first-episode schizophrenia. *Biol. Psychiatry* 45(10): 1321–1328.
- 524 503 Dryden I.L., Mardia K.V., 2016. *Statistical shape analysis, with applications in R: Second edition.*
- 525 504 Gower J.C., 1975. Generalized procrustes analysis. *Psychometrika* 40(1): 33-51.
- 526 505 Jungers W.L., Falsetti A.B., Wall C.E., 1995. Shape, relative size, and size- adjustments in
527 506 morphometrics. *Am. J. Phys. Anthropol.* 38(S21): 137–161.
- 528 507 Kendall D.G., 1977. The diffusion of shape. *Adv. Appl. Probab.* 9(3): 428–430.
- 529 508 Klingenberg C.P., 2013. Visualizations in geometric morphometrics: how to read and how to make
530 509 graphs showing shape changes. *Hystrix, Ital. J. Mammal.* 24(1): 15–24.
- 531 510 Klingenberg C.P., McIntyre G.S., Zaklan S.D., 1998. Left-right asymmetry of fly wings and the
532 511 evolution of body axes. *Proc. R. Soc. B Biol. Sci.* 265(1402): 1255-1259.
- 533 512 Mallison H., Wings O., 2014. Photogrammetry in paleontology—a practical guide. *J. Paleontol. Tech.*

- 535 513 Meloro C., Cáceres N.C., Carotenuto F., Sponchiado J., Melo G.L., Passaro F., Raia P., 2015.
536 514 Chewing on the trees: Constraints and adaptation in the evolution of the primate mandible.
537 515 *Evolution* 69(7): 1690-1700.
- 538 516 Meloro C., Hunter J., Tomsett L., Portela Miguez R., Prevosti F.J., Brown R.P., 2017. Evolutionary
539 517 ecomorphology of the Falkland Islands wolf *Dusicyon australis*. *Mamm. Rev.* 47(2): 159–163.
- 540 518 Mullin S.K., Taylor P.J., 2002. The effects of parallax on geometric morphometric data. *Comput.*
541 519 *Biol. Med.* 32(6): 455–464.
- 542 520 Neaux D., Sansalone G., Ledogar J.A., Ledogar S.H., Luk T.H.Y., Wroe S., 2018. Basicranium and
543 521 face: Assessing the impact of morphological integration on primate evolution. *J. Hum. Evol.*
544 522 118: 43–55.
- 545 523 Olsen A.M., Westneat M.W., 2015. StereoMorph: An R package for the collection of 3D landmarks
546 524 and curves using a stereo camera set-up. *Methods Ecol. Evol.* 6(3): 351-356.
- 547 525 Owen M., Provan J.S., 2011. A fast algorithm for computing geodesic distances in tree space.
548 526 *IEEE/ACM Trans. Comput. Biol. Bioinforma.* 8(1): 2–13.
- 549 527 Piras P., Buscalioni A.D., Teresi L., Raia P., Sansalone G., Kotsakis T., Cubo J., 2014. Morphological
550 528 integration and functional modularity in the crocodylian skull. *Integr. Zool.* 9(4): 498–516.
- 551 529 Piras P., Marcolini F., Raia P., Curcio M., Kotsakis T., 2010. Ecophenotypic variation and
552 530 phylogenetic inheritance in first lower molar shape of extant Italian populations of *Microtus*
553 531 (*Terricola*) *savii* (Rodentia). *Biol. J. Linn. Soc.* 99(3): 632–647.
- 554 532 Piras P., Teresi L., Buscalioni A.D., Cubo J., 2009. The shadow of forgotten ancestors differently
555 533 constrains the fate of Alligatoidea and Crocodyloidea. *Glob. Ecol. Biogeogr.* 18(1): 30–40.
- 556 534 Piras P., Teresi L., Traversetti L., Varano V., Gabriele S., Kotsakis T., Raia P., Puddu P.E., Scalici
557 535 M., 2016. The conceptual framework of ontogenetic trajectories: Parallel Transport allows the
558 536 recognition and visualization of pure deformation patterns. *Evol. Dev.* 18(3): 182–200.

- 560 537 Ponton D., 2006. Is geometric morphometrics efficient for comparing otolith shape of different fish
561 538 species? *J. Morphol.* 267(6): 750–757.
- 562 539 Profico A., Bellucci L., Buzi C., Di Vincenzo F., Micarelli I., Strani F., Tafuri M.A., Manzi G.,
563 540 2018a. Virtual anthropology and its application in cultural heritage studies. *Stud. Conserv.*
564 541 64(6):1–14.
- 565 542 Profico A., Schlager S., Valoriani V., Buzi C., Melchionna M., Veneziano A., Raia P., Moggi-Cecchi
566 543 J., Manzi G., 2018b. Reproducing the internal and external anatomy of fossil bones: two new
567 544 automatic digital tools. *Am. J. Phys. Anthropol.* 166(4): 979-986.
- 568 545 Profico A., Veneziano A., Buzi C., Melchionna M., Raia P., 2019. Geometric Morphometrics
569 546 Analyses. <https://github.com/Arothron>.
- 570 547 Rohlf F.J., 2000. On the use of shape spaces to compare morphometric methods. *Hystrix-the Ital. J.*
571 548 *Mammal.* 11(1): 9-25.
- 572 549 Rohlf F.J., Corti M., 2000. Use of two-block partial least-squares to study covariation in shape. *Syst.*
573 550 *Biol.* 49(4): 740–753.
- 574 551 Rohlf F.J., Marcus L.F., 1993. A revolution morphometrics. *Trends Ecol. Evol.* 8(4): 129–132.
- 575 552 Sansalone G., Kotsakis T., Piras P., 2015. *Talpa fossilis* or *Talpa europaea*? Using geometric
576 553 morphometrics and allometric trajectories of humeral moles remains from Hungary to answer a
577 554 taxonomic debate. *Palaeontol. Electron.* 18(2): 1–17.
- 578 555 Sokal R.R., Michener C., 1958. A statistical method for evaluating systematic relationships.
- 579 556 Varano V., Gabriele S., Teresi L., Dryden I.L., Puddu P.E., Torromeo C., Piras P., 2017. The TPS
580 557 Direct Transport: A New Method for Transporting Deformations in the Size-and-Shape Space.
581 558 *Int. J. Comput. Vis.* 124(3): 384-408.
- 582 559 Varano V., Piras P., Gabriele S., Teresi L., Nardinocchi P., Dryden I.L., Torromeo C., Puddu P.E.,
583 560 2018. The decomposition of deformation: New metrics to enhance shape analysis in medical

- 585 561 imaging. *Med. Image Anal.* 46: 35–56.
- 586 562 Veneziano A., Landi F., Profico A., 2018. Surface smoothing, decimation, and their effects on 3D
587 563 biological specimens. *Am. J. Phys. Anthropol.* 166(2): 473-480.
- 588 564 Viscosi V., Cardini A., 2011. Leaf morphology, taxonomy and geometric morphometrics: A
589 565 simplified protocol for beginners. *PLoS One* 6(10): e25630.
- 590 566 Weber G.W., 205. Virtual anthropology. *Am. J. Phys. Anthropol.* 156(S59): 22–42.
- 591 567
- 592 568
- 593 569

595 570 **TABLES:**

596 571 Table 1: Procrustes distances calculated between 2D projections of shapes predicted at extremes of the first two
 597 572 PC scores of 3D data and corresponding 2D shapes predicted by the PCA performed on the combined 2D dataset
 598 573 with (our method) and without size correction. We reported the values for the two shapes (“Irregular” and
 599 574 “Circular” shapes).

	PC1 min		PC1 max		PC2 min		PC2 max	
	Irregular shape	Circular shape	Irregular shape	Circular shape	Irregular shape	Circular shape	Irregular shape	Circular shape
603 604 With size correction	0.0108	0.0010	0.0090	0.0007	0.0114	0.0001	0.0103	0.0007
605 606 607 Without size correction	0.0105	0.0630	0.0111	0.0087	0.3718	0.1347	0.3747	0.1346

608 575

609 576

610 577 Table 2: Geodesic and edge set distances calculated between the clustered tree of the 3D data and the 2D data.
 611 578 We considered the trees built taking into account all the specimens, the values pooled by species and the values
 612 579 pooled by species and gender. We reported the average values for 2D combined views. We replicated the analyses
 613 580 with and without the size correction.

614 581

N. of views	Geodesic	Edge set	Geodesic	Edge set
	No size correction		With size correction	
617 1	3.18%	103.33	3.18%	103.33
618 2	2.81%	91.53	2.54%	84.20
619 3	2.61%	83.75	2.34%	74.85
620 4	2.61%	79.06	2.27%	67.73
621 5	2.59%	75.00	2.22%	65.67
622 6	2.77%	80.00	2.09%	59.00

623 582

624 583

625 584

626 585

628 586

629 587 Table 3. First 5 axes of covariation with percentage of the explained covariance (% cov), coefficient of correlation

630 588 (Corr. Coeff.) and *p*-values calculated by performing the PLS between the PC scores coming from the 3D and

631 589 2Dcomp data with and without correction.

PLS axis	No size correction			With size correction		
	% cov.	Corr. Coeff.	p-value	% cov.	Corr. Coeff.	p-value
PLS 1	55.551	0.995	0.001	55.551	0.995	0.001
PLS 2	25.248	0.994	0.001	25.074	0.997	0.001
PLS 3	15.964	0.991	0.001	16.462	0.994	0.001
PLS 4	1.308	0.975	0.001	1.301	0.984	0.001
PLS 5	0.380	0.961	0.001	0.376	0.980	0.001

639 590

640 591 Table 4: The Mantel test performed between the shape information encoded in 3D data and in combined 2D data

641 592 with and without size correction. The average values for Z-statistic combining two, three, four, five and six 2D

642 593 views are reported.

643 594

N. of views	No size correction		With size correction	
	Z-statistic	p-value	Z-statistic	p-value
2	0.90	0.01	0.91	0.01
3	0.93	0.01	0.95	0.01
4	0.96	0.01	0.97	0.01
5	0.97	0.01	0.98	0.01
6	0.98	0.01	0.99	0.01

651 596

652 597

653 598

654 599

Table 5: Procrustes Anova results performed on 3D and 2D combined datasets (with and without “size correction”) defining the centroid size vector of 3D data as regressor. We applied the Procrustes Anova on three different groups: Platyrrhini, Cercopithecoidea and Hominoidea.

	3D data		Combined 2D data (with size correction)		Combined 2D data (without size correction)	
	R-squared	P-value	R-squared	P-value	R-squared	P-value
Platyrrhini	0.459	0.001	0.434	0.001	0.437	0.001
Cercopithecoidea	0.390	0.001	0.389	0.001	0.397	0.001
Hominoidea	0.352	0.001	0.304	0.001	0.305	0.001

Table 6: Geodesic and edge set distance calculated between UPGMA trees of the 3D data and 2D data with and without size correction. We report also the distances pooling the data by species and sex.

PC scores	Geodesic distance		Edge set distance	
	No size correction	With size correction	No size correction	With size correction
No pooled	2.47%	2.09%	69	59
Pooled by species	1.82%	1.34%	0	0
Pooled by species and sex	2.50%	2.19%	1	1

FIGURE LEGENDS:

Figure 1. Protocol used to convert a 3D landmark configuration into six different 2D sets. The midsagittal (in green) and Frankfurt (in red) planes are reported on a *Macaca arctoides* 3D model (A). The visible triangles (B) of the mesh and the visible landmarks (C) from the point of view set on superior view are reported in red and blue respectively. 2D landmark set with wireframe of a specimen of *Macaca arctoides* in superior view (D).

Figure 2. The “combinland” method. Landmarks are recorded separately on different anatomical views (A). GPA is performed on each 2D datasets (B). The 2D sets after GPA are corrected by the square root of the number of

689 619 landmarks times the number of dimensions of each set (red and green: before and after correction, respectively)
690 620 (C). Merging of the corrected coordinates (2D datasets) and PCA on the new matrix of coordinates (D).

691 621
692 622 Figure 3. Biplots showing the relation between Centroid Size (CS) and number of landmarks (k) (A). In this
693 623 example, the structure (a single circle of radius = 1) is the same in all of the 10 configurations (where B and C are
694 624 two examples). On the right the relation between Centroid Size (CS) and distance from centroid (D) is shown. In
695 625 this example, the structures (two concentric circles) has been digitalized using the same number of landmarks (for
696 626 a total of 42): the external circles have the same radius ($r = 1$) in all the configurations while the internal ones are
697 627 progressively scaled (e.g. E and F, the range of the radii for the internal circles, r_i is bracketed between 0.1 and
698 628 0.9). The vertical line shows the CS values of the structure without the inner circle.

699 629
700 630 Figure 4. Experiment: simulated datasets (for a total of 300 specimens) consisting of two hypothetical anatomical
701 631 views that possess exactly the same circular shape. The first one (F) is defined by 10 landmarks, the second one
702 632 (S) is defined digitalizing 100 landmarks. On the right the two CS corrections are reported. The relative CS after
703 633 the correction published by Davis and colleagues (2016) is shown as red (F view) and violet (S view) lines. The
704 634 relative CS after the application of the correction proposed in this work is reported in blue (F view) and green (S
705 635 view).

706 636
707 637 Figure 5 Plot of the first undeformed specimen belonging to the simulated case study. On the left column the
708 638 two 2D-landmark configurations (irregular and circular shapes); these configurations refer to shapes that possess
709 639 approximately the same physical size. On the middle the combined 3D landmark configuration shown on XY
710 640 and XZ axes. On the top right the full combined 3D dataset consisting on the deformation of the first shape after
711 641 Procrustes registration. The 3D landmark configuration is also shown (bottom right).

712 642 Figure 6 PCA plots performed on the 3D original landmark configuration (top left) and on the 2D combined
713 643 landmark configurations without (top right) and with (bottom left) size correction. At bottom right, the relative
714 644 sizes of the two 2D combined datasets compared to the entire configuration resulting by merging them in a
715 645 single shape. Only the size-corrected configurations (red dots) appear insensitive to the number of landmarks
716 646 per configuration thus returning similar CS values. The same does not apply for non-corrected configurations
717 647 (green dots) that give green values approximately four times greater than the red ones.

[Download source file \(111.24 kB\)](#)

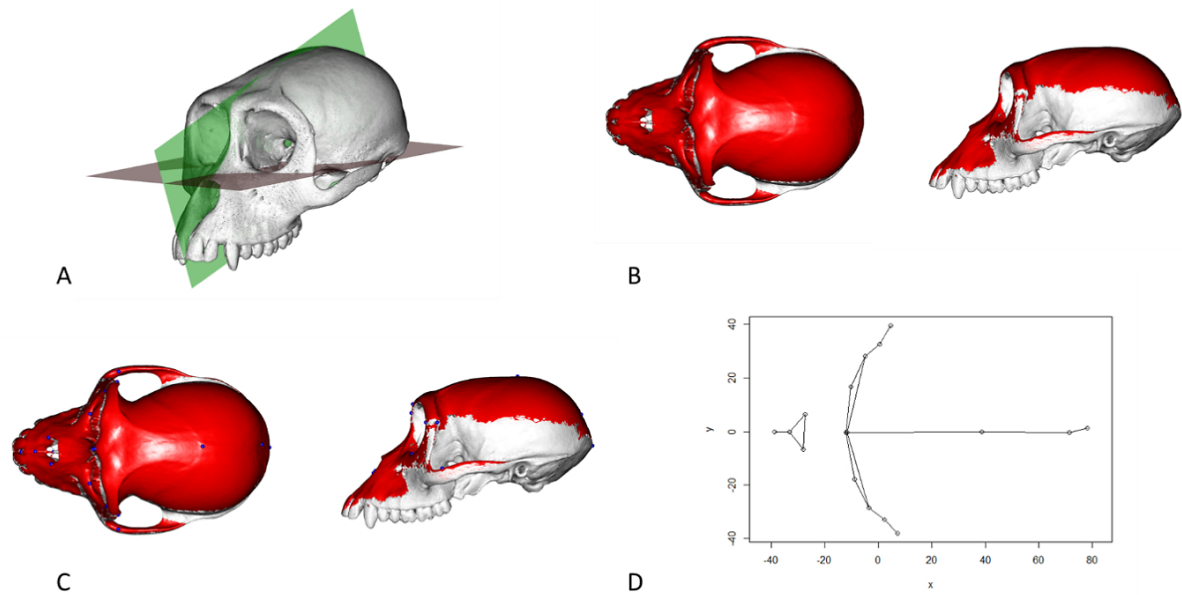
719 648 Figure 7. Shape variations associated at the extremes of the first two principal components for 3D and 2D
720 649 combined datasets (with and without size correction). For saving space we reported in the same panel the two
721 650 shape variations of 2D combined data predicted by PC extreme values associated to the irregular and circular
722 651 shapes. The first two rows show the shape variations of 3D data, i.e. the irregular and circular shapes, the third
723 652 row the shape variations corresponding to the combined 2D data without size correction (circular and irregular
724 653 shapes on the same panel), the fourth row the shape variation of the combined 2D data with size correction
725 654 (circular and irregular shapes on the same panel). It can be seen that a drastic size bias is present in the third row.

726 655
727 656 Figure 8. Cumulative variance explained by the first 5 PCs in the 3D (left) and combined 2D (right) data. The
728 657 percentage of variance explained by each of the first 5 PCs is reported in the plot.

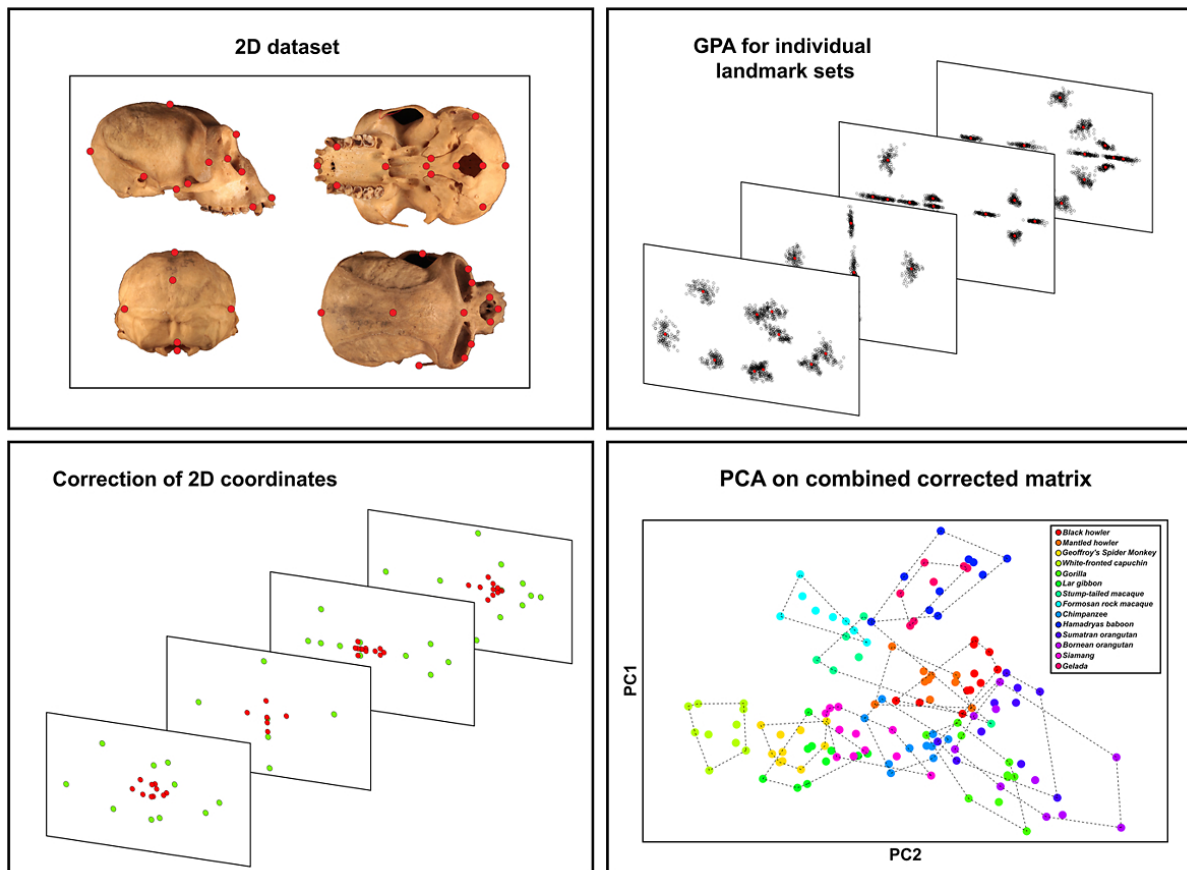
729 658
730 659 Figure 9. Plot of the first two PCs of the 3D (left) and combined 2D Primate data (right). A convex hull encloses
731 660 each species: *Alouatta caraya* in red, *Alouatta palliata* in orange, *Ateles geoffrey* in gold, *Cebus albifrons* in yellow
732 661 green, *Gorilla gorilla* in green, *Hylobates lar* in dark green, *Macaca arctoides* in light blue, *Macaca cyclops* in
733 662 cyan, *Pan troglodytes* in light sky blue, *Papio hamadryas* in blue, *Pongo abelii* in slate blue, *Pongo pygmaeus* in
734 663 violet, *Symphalangus syndactylus* in fuchsia and *Theropithecus gelada* in magenta.

735 664
736 665 Figure 10. Shape variations associated to negative (red) and positive (blue) extreme values of the first two
737 666 principal components for the 3D and combined 2D data.

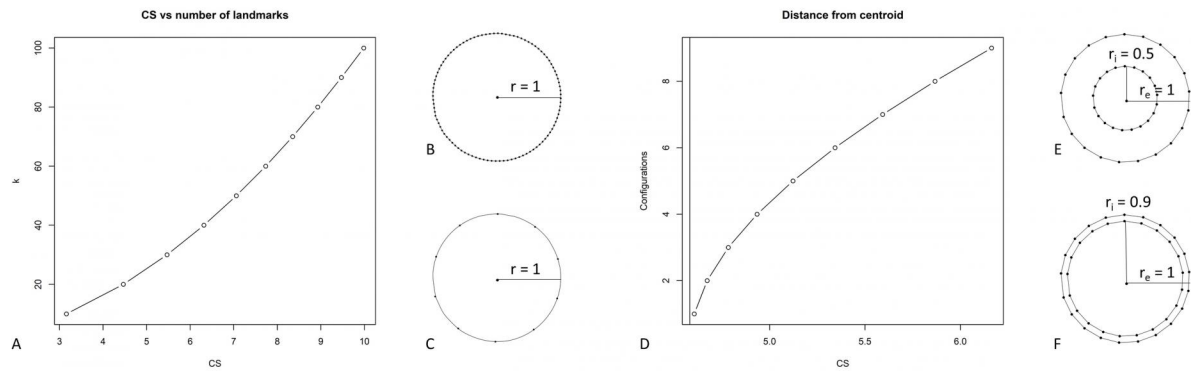
738 667
739 668 Figure 11. Upper row: comparison of the shape variation coming from 3D and 2D datasets (right-lateral view).
740 669 Plot of the Cartesian coordinates associated with the minimum and maximum values of the PC1 in right-lateral
741 670 view (A and B, 3D data in green and 2D data in red). Bottom left: PCA plot of the shape variations coming from
742 671 3D and 2D data (3D data in green and 2D data in red) combined together. Bottom right: scatterplot matrix
743 672 performed on the eigenvectors (3D and 2D data) referred to the first three PCs (D) and coming from separate
744 673 PCA.



Protocol used to convert a 3D landmark configuration into six different 2D sets. The midsagittal (in green) and Frankfurt (in red) planes are reported on a *Macaca arctoides* 3D model (A). The visible triangles (B) of the mesh and the visible landmarks (C) from the point of view set on superior view are reported in red and blue respectively. 2D landmark set with wireframe of a specimen of *Macaca arctoides* in superior view (D).



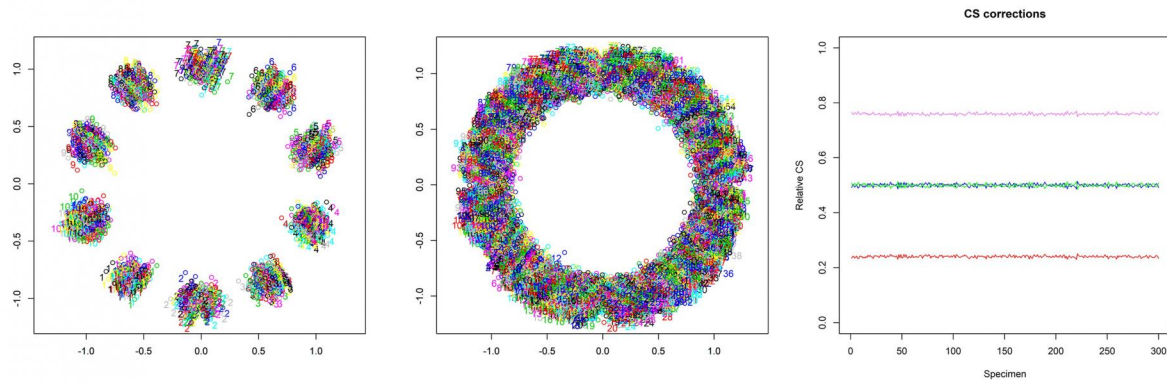
The “combinland” method. Landmarks are recorded separately on different anatomical views (A). GPA is performed on each 2D datasets (B). The 2D sets after GPA are corrected by the square root of the number of landmarks times the number of dimensions of each set (red and green: before and after correction, respectively) (C). Merging of the corrected coordinates (2D datasets) and PCA on the new matrix of coordinates (D).



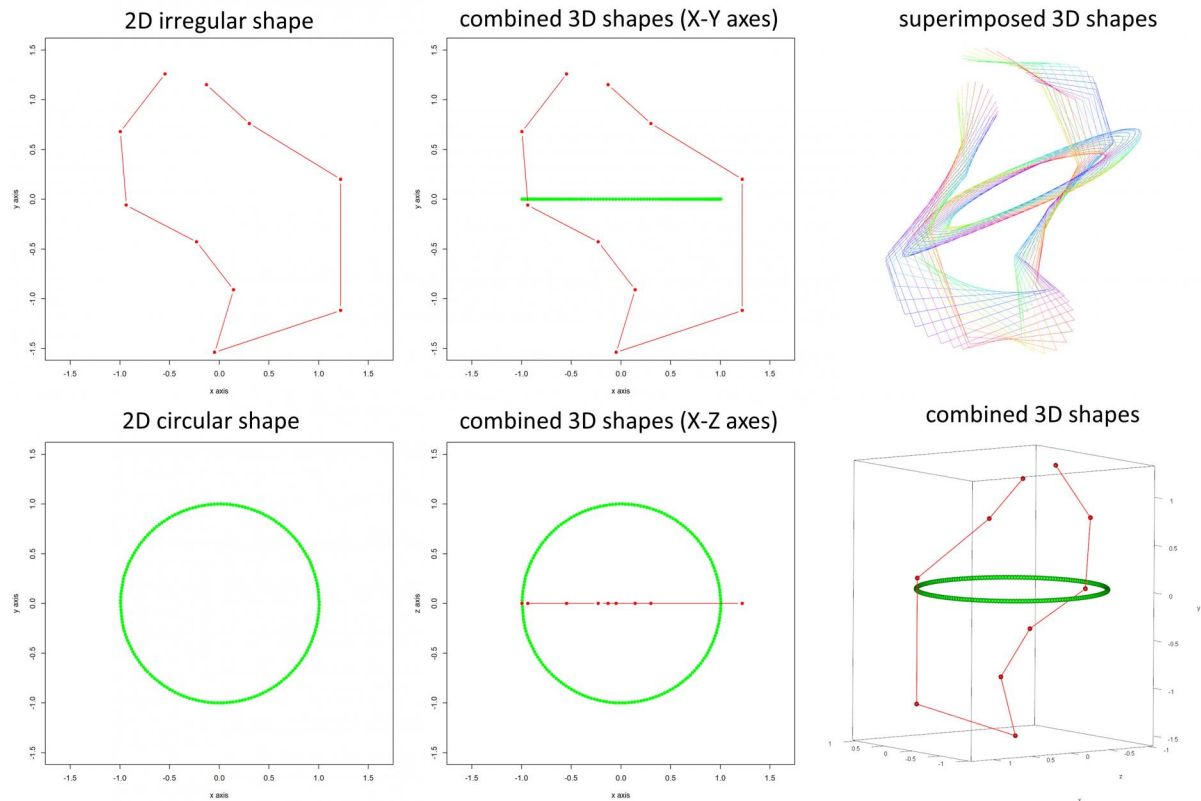
Biplots showing the relation between Centroid Size (CS) and number of landmarks (k) (A). In this example, the structure (a single circle of radius = 1) is the same in all of the 10 configurations (where B and C are two examples). On the right the relation between Centroid Size (CS) and distance from centroid (D) is shown. In this example, the structures (two concentric circles) has been digitalized using the same number of landmarks (for a total of 42): the external circles have the same radius ($r = 1$) in all the configurations while the internal ones are progressively scaled (e.g. E and F, the range of the radii for the internal circles, r_i , is bracketed between 0.1 and 0.9). The vertical line shows the CS values of the structure without the inner circle.

Figure 4

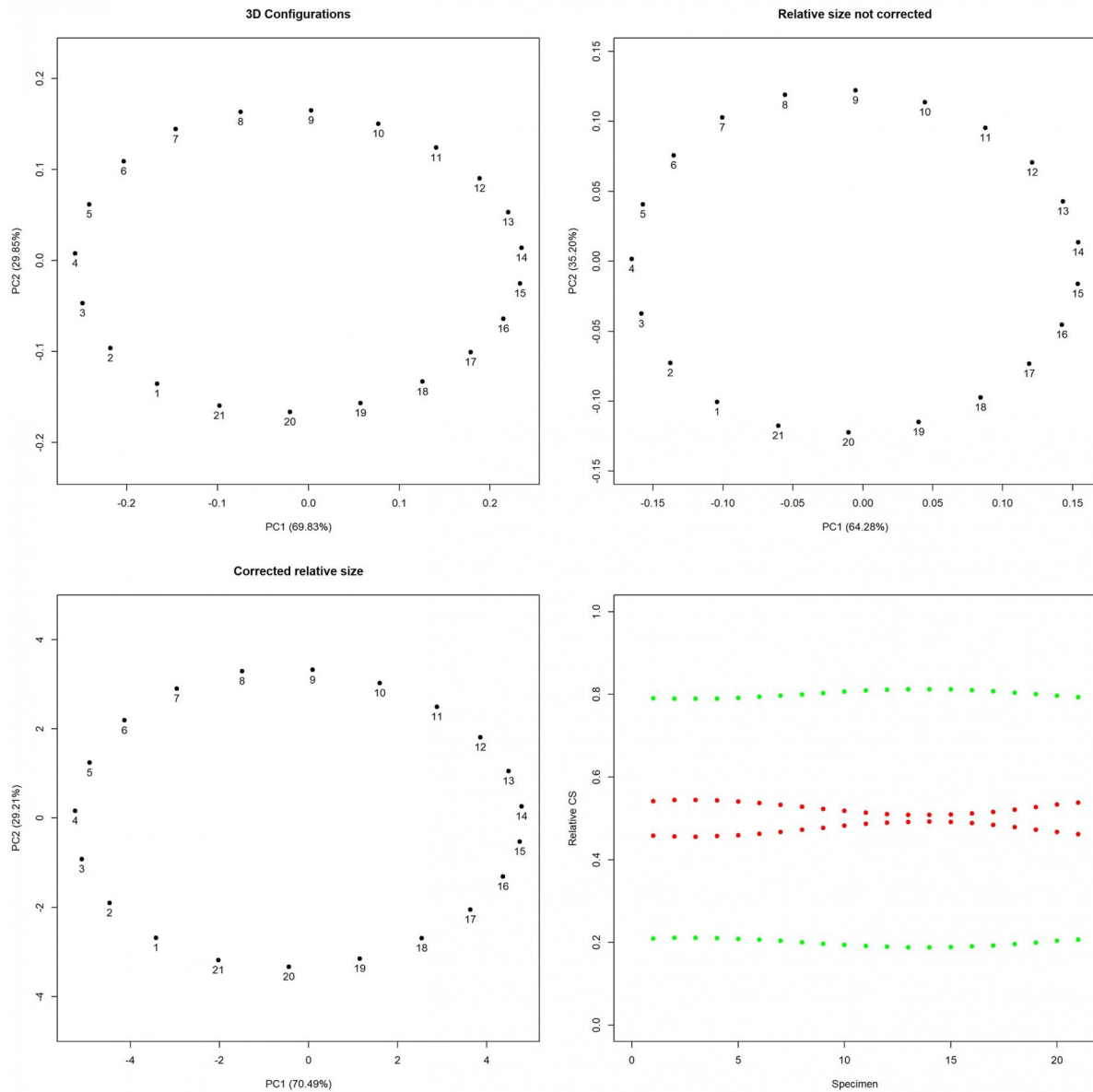
[Download source file \(703.25 kB\)](#)



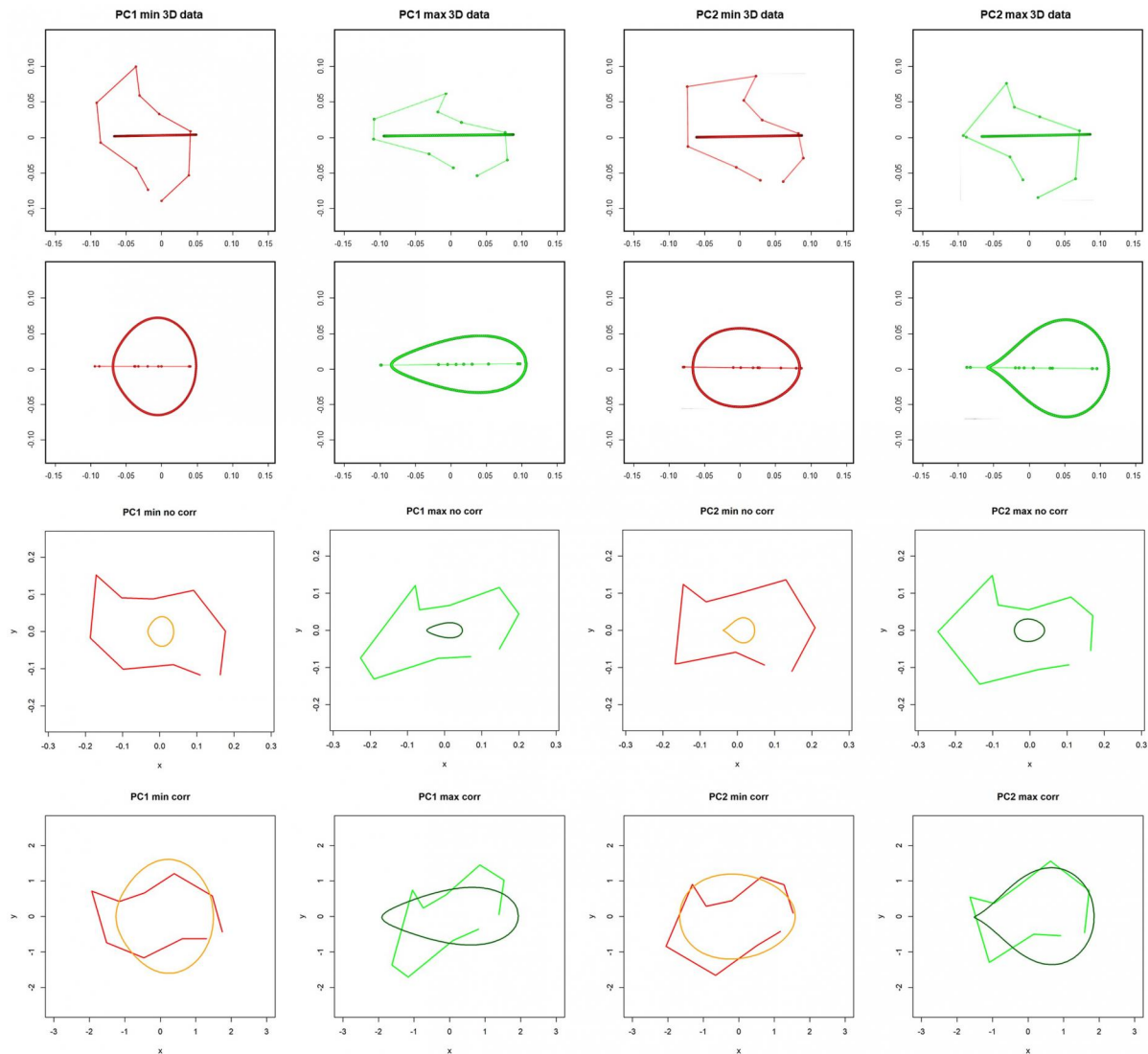
Experiment: simulated datasets (for a total of 300 specimens) consisting of two hypothetical anatomical views that possess exactly the same circular shape. The first one (F) is defined by 10 landmarks, the second one (S) is defined digitalizing 100 landmarks. On the right the two CS corrections are reported. The relative CS after the correction published by Davis and colleagues (2016) is shown as red (F view) and violet (S view) lines. The relative CS after the application of the correction proposed in this work is reported in blue (F view) and green (S view).



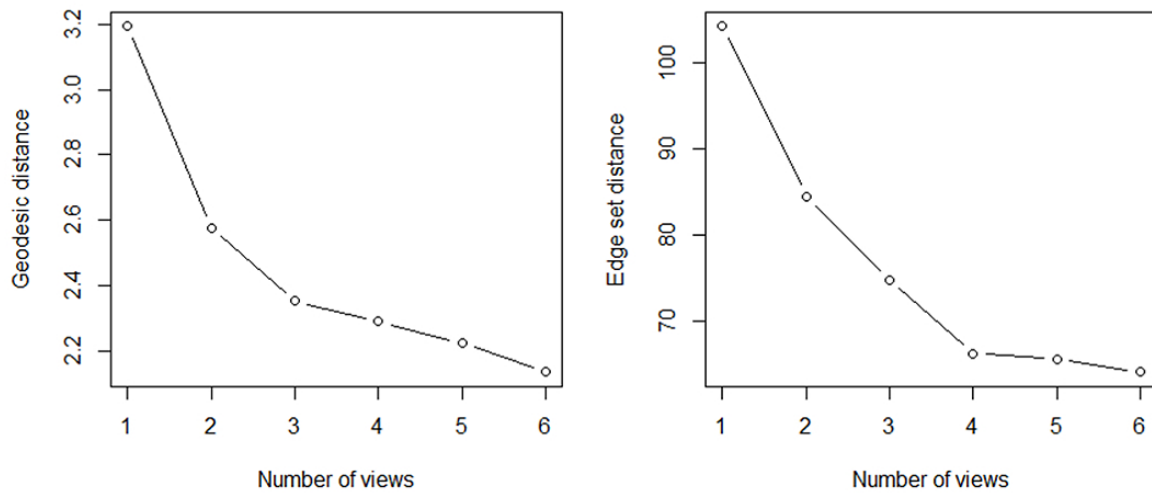
Plot of the first undeformed specimen belonging to the simulated case study. On the left column the two 2D-landmark configurations (irregular and circular shapes); these configurations refer to shapes that possess approximately the same physical size. On the middle the combined 3D landmark configuration shown on XY and XZ axes. On the top right the full combined 3D dataset consisting on the deformation of the first shape after Procrustes registration. The 3D landmark configuration is also shown (bottom right).



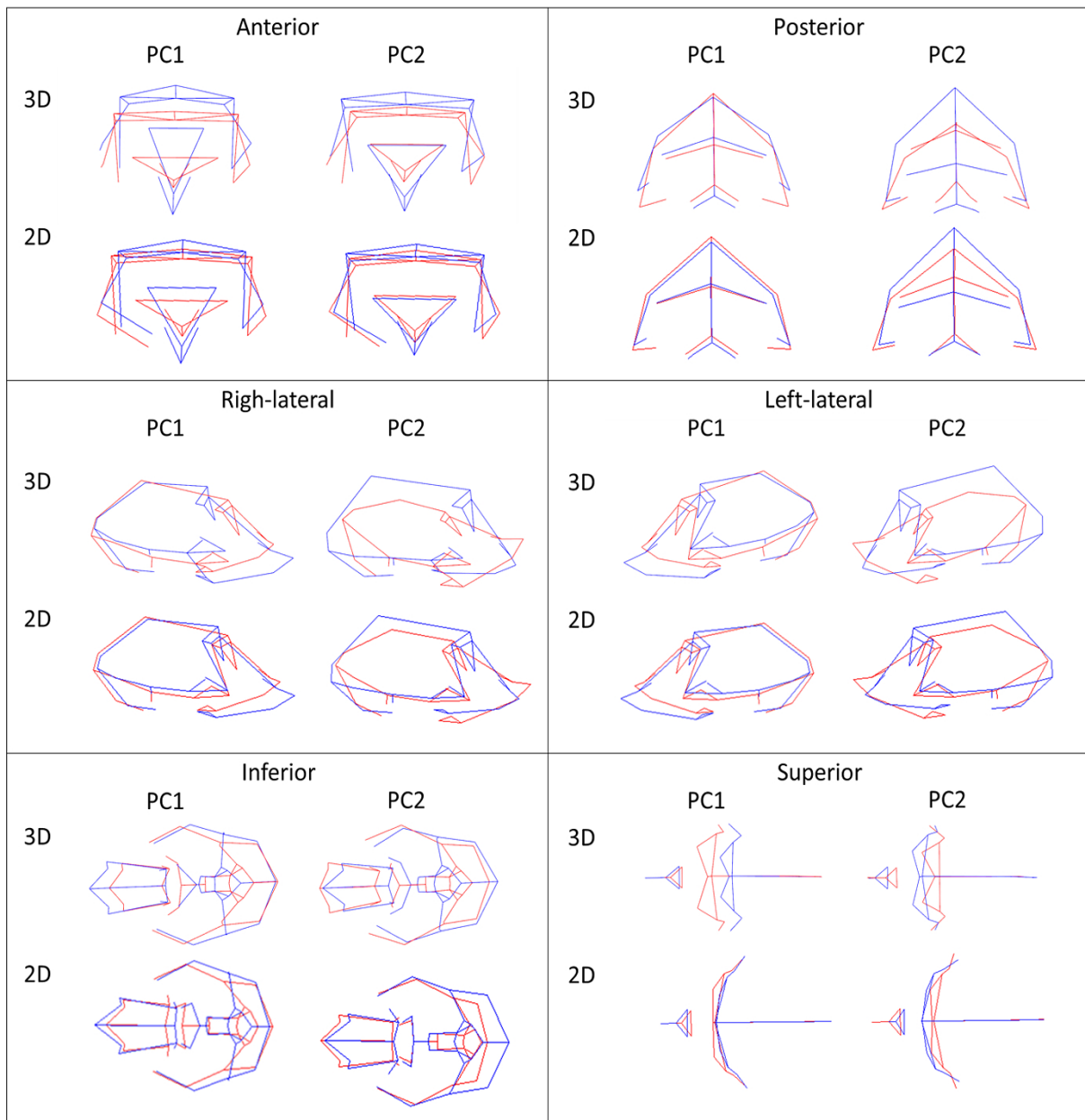
PCA plots performed on the 3D original landmark configuration (top left) and on the 2D combined landmark configurations without (top right) and with (bottom left) size correction. At bottom right, the relative sizes of the two 2D combined datasets compared to the entire configuration resulting by merging them in a single shape. Only the size-corrected configurations (red dots) appear insensitive to the number of landmarks per configuration thus returning similar CS values. The same does not apply for non-corrected configurations (green dots) that give green values approximately four times greater than the red ones.



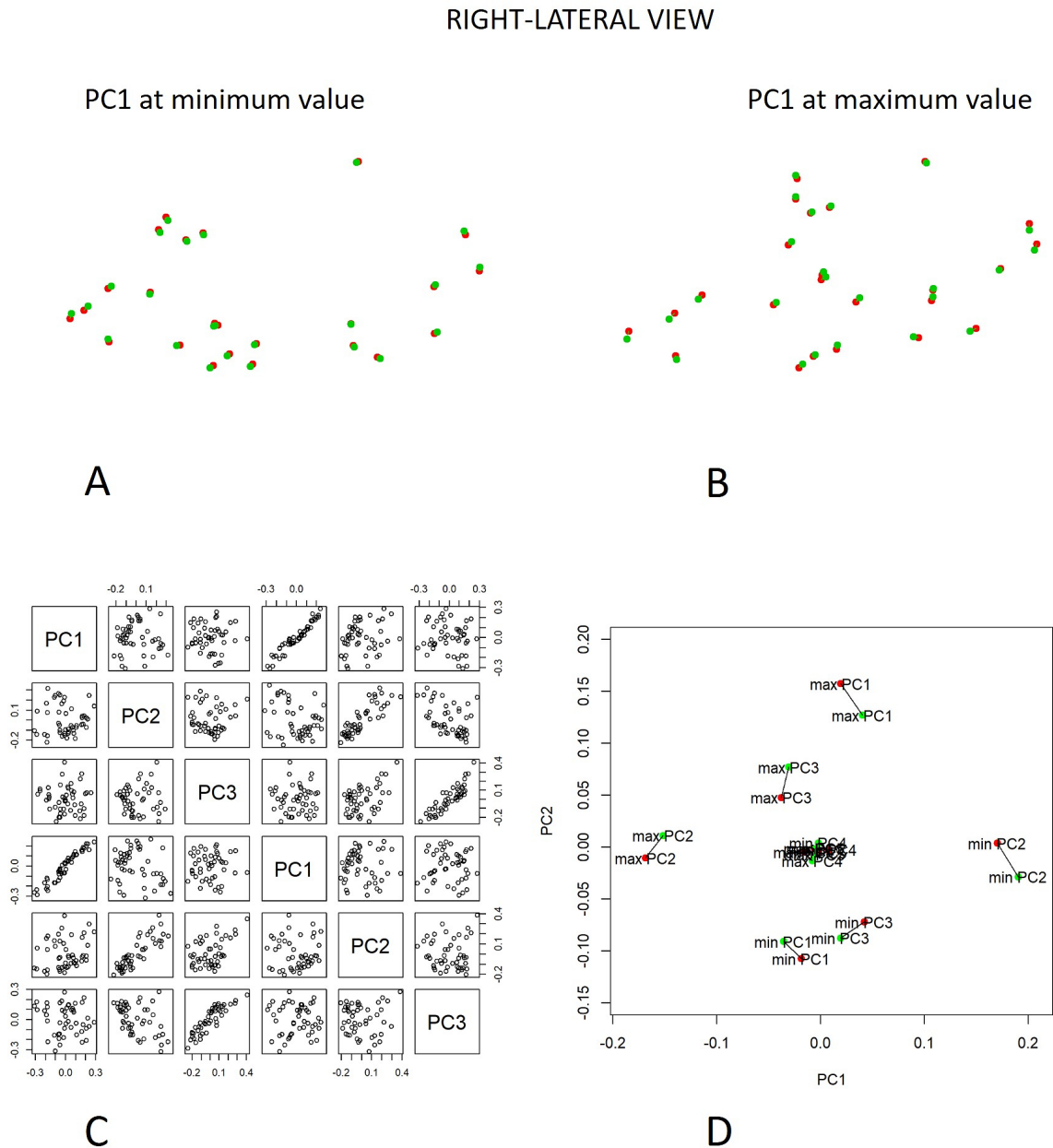
Shape variations associated at the extremes of the first two principal components for 3D and 2D combined datasets (with and without size correction). For saving space we reported in the same panel the two shape variations of 2D combined data predicted by PC extreme values associated to the irregular and circular shapes. The first two rows show the shape variations of 3D data, i.e. the irregular and circular shapes, the third row the shape variations corresponding to the combined 2D data without size correction (circular and irregular shapes on the same panel), the fourth row the shape variation of the combined 2D data with size correction (circular and irregular shapes on the same panel). It can be seen that a drastic size bias is present in the third row.



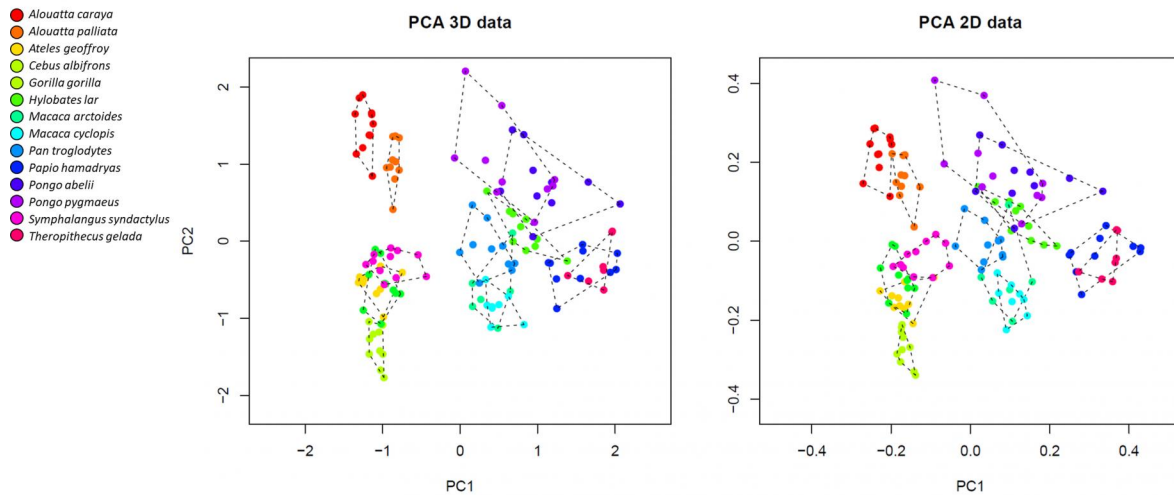
Cumulative variance explained by the first 5 PCs in the 3D (left) and combined 2D (right) data. The percentage of variance explained by each of the first 5 PCs is reported in the plot.



Shape variations associated to negative (red) and positive (blue) extreme values of the first two principal components for the 3D and combined 2D data.



Upper row: comparison of the shape variation coming from 3D and 2D datasets (right-lateral view). Plot of the Cartesian coordinates associated with the minimum and maximum values of the PC1 in right-lateral view (A and B, 3D data in green and 2D data in red). Bottom left: PCA plot of the shape variations coming from 3D and 2D data (3D data in green and 2D data in red) combined together. Bottom right: scatterplot matrix performed on the eigenvectors (3D and 2D data) referred to the first three PCs (D) and coming from separate PCA.



Plot of the first two PCs of the 3D (left) and combined 2D Primate data (right). A convex hull encloses each species: *Alouatta caraya* in red, *Alouatta palliata* in orange, *Ateles geoffroy* in gold, *Cebus albifrons* in yellow green, *Gorilla gorilla* in green, *Hylobates lar* in dark green, *Macaca arctoides* in light blue, *Macaca cyclopis* in cyan, *Pan troglodytes* in light sky blue, *Papio hamadryas* in blue, *Pongo abelii* in slate blue, *Pongo pygmaeus* in violet, *Symphalangus syndactylus* in fuchsia and *Theropithecus gelada* in magenta.

Manuscript body

[Download source file \(111.24 kB\)](#)

Figures

Figure 1 - [Download source file \(465.51 kB\)](#)

Protocol used to convert a 3D landmark configuration into six different 2D sets. The midsagittal (in green) and Frankfurt (in red) planes are reported on a *Macaca arctoides* 3D model (A). The visible triangles (B) of the mesh and the visible landmarks (C) from the point of view set on superior view are reported in red and blue respectively. 2D landmark set with wireframe of a specimen of *Macaca arctoides* in superior view (D).

Figure 2 - [Download source file \(506.1 kB\)](#)

The “combinland” method. Landmarks are recorded separately on different anatomical views (A). GPA is performed on each 2D datasets (B). The 2D sets after GPA are corrected by the square root of the number of landmarks times the number of dimensions of each set (red and green: before and after correction, respectively) (C). Merging of the corrected coordinates (2D datasets) and PCA on the new matrix of coordinates (D).

Figure 3 - [Download source file \(290.28 kB\)](#)

Biplots showing the relation between Centroid Size (CS) and number of landmarks (k) (A). In this example, the structure (a single circle of radius = 1) is the same in all of the 10 configurations (where B and C are two examples). On the right the relation between Centroid Size (CS) and distance from centroid (D) is shown. In this example, the structures (two concentric circles) has been digitalized using the same number of landmarks (for a total of 42): the external circles have the same radius ($r = 1$) in all the configurations while the internal ones are progressively scaled (e.g. E and F, the range of the radii for the internal circles, r_i is bracketed between 0.1 and 0.9). The vertical line shows the CS values of the structure without the inner circle.

Figure 4 - [Download source file \(703.25 kB\)](#)

Experiment: simulated datasets (for a total of 300 specimens) consisting of two hypothetical anatomical views that possess exactly the same circular shape. The first one (F) is defined by 10 landmarks, the second one (S) is defined digitalizing 100 landmarks. On the right the two CS corrections are reported. The relative CS after the correction published by Davis and colleagues (2016) is shown as red (F view) and violet (S view) lines. The relative CS after the application of the correction proposed in this work is reported in blue (F view) and green (S view).

Figure 5 - [Download source file \(1.11 MB\)](#)

Plot of the first undeformed specimen belonging to the simulated case study. On the left column the two 2D-landmark configurations (irregular and circular shapes); these configurations refer to shapes that possess approximately the same physical size. On the middle the combined 3D landmark configuration shown on XY and XZ axes. On the top right the full combined 3D dataset consisting on the deformation of the first shape after Procrustes registration. The 3D landmark configuration is also shown (bottom right).

Figure 6 - [Download source file \(293.73 kB\)](#)

PCA plots performed on the 3D original landmark configuration (top left) and on the 2D combined landmark configurations without (top right) and with (bottom left) size correction. At bottom right, the relative sizes of the two 2D combined datasets compared to the entire configuration resulting by merging them in a single shape. Only the size-corrected configurations (red dots) appear insensitive to the number of landmarks per configuration thus returning similar CS values. The same does not apply for non-corrected configurations (green dots) that give green values approximately four times greater than the red ones.

Figure 7 - [Download source file \(475.2 kB\)](#)

Shape variations associated at the extremes of the first two principal components for 3D and 2D combined datasets (with and without size correction). For saving space we reported in the same panel the two shape variations of 2D combined data predicted by PC extreme values associated to the irregular and circular shapes. The first two rows show the shape variations of 3D data, i.e. the irregular and circular shapes, the third row the shape variations corresponding to the combined 2D data without size correction (circular and irregular shapes on the same panel), the fourth row the shape variation of the combined 2D data with size correction (circular and irregular shapes on the same panel). It can be seen that a drastic size bias is present in the third row.

Figure 8 - [Download source file \(132.43 kB\)](#)

Cumulative variance explained by the first 5 PCs in the 3D (left) and combined 2D (right) data. The percentage of variance explained by each of the first 5 PCs is reported in the plot.

Figure 9 - [Download source file \(682.32 kB\)](#)

Shape variations associated to negative (red) and positive (blue) extreme values of the first two principal components for the 3D and combined 2D data.

Figure 10 - [Download source file \(328.77 kB\)](#)

Upper row: comparison of the shape variation coming from 3D and 2D datasets (right-lateral view). Plot of the Cartesian coordinates associated with the minimum and maximum values of the PC1 in right-lateral view (A and B, 3D data in green and 2D data in red). Bottom left: PCA plot of the shape variations coming from 3D and 2D data (3D data in green and 2D data in red) combined together. Bottom right: scatterplot matrix performed on the eigenvectors (3D and 2D data) referred to the first three PCs (D) and coming from separate PCA.

Figure 11 - [Download source file \(996.74 kB\)](#)

Plot of the first two PCs of the 3D (left) and combined 2D Primate data (right). A convex hull encloses each species: *Alouatta caraya* in red, *Alouatta palliata* in orange, *Ateles geoffrey* in gold, *Cebus albifrons* in yellow green, *Gorilla gorilla* in green, *Hylobates lar* in dark green, *Macaca arctoides* in light blue, *Macaca cyclopis* in cyan, *Pan troglodytes* in light sky blue, *Papio hamadryas* in blue, *Pongo abelii* in slate blue, *Pongo pygmaeus* in violet, *Symphalangus syndactylus* in fuchsia and *Theropithecus gelada* in magenta.

Supplementary Online Material

[Download source file \(5.25 MB\)](#)